Nonlocal quantum gate on quantum continuous variables with minimal resources

Shota Yokoyama,[1,*] Ryuji Ukai,[1] Jun-ichi Yoshikawa,[1] Petr Marek,[2] Radim Filip,[2] and Akira Furusawa[1,†]

[1]*Department of Applied Physics, School of Engineering, The University of Tokyo, 7-3-1 Hongo, Bunkyo-ku, Tokyo 113-8656, Japan*

[2]*Department of Optics, Palacký University, 17. Listopadu 1192/12, 771 46 Olomouc, Czech Republic*

(Received 14 March 2014; published 8 July 2014)

We experimentally demonstrate, with an all-optical setup, a nonlocal deterministic quantum nondemolition interaction gate applicable to quantum states at nodes separated by a physical distance and connected by classical communication channels. The gate implementation, based on entangled states shared in advance, local operations, and classical communication, runs completely in parallel fashion at both of the local nodes, requiring minimum resources. The nondemolition character of the gate up to the local unitary squeezing is verified by the analysis using several coherent states. A genuine quantum nature of the gate is confirmed by the capability of deterministically producing an entangled state at the output from two separable input states. The all-optical nonlocal gate operation can be potentially incorporated into distributed quantum computing with atomic or solid-state systems as a cross-processor unitary operation.

DOI: 10.1103/PhysRevA.90.012311 PACS number(s): 03.67.Lx, 42.50.Ex, 42.65.−k

I. INTRODUCTION

A quantum computer is a powerful machine, capable of solving several important problems much faster than existing computers [1,2]. Currently, atomic or solid-state quantum systems are candidates for feasible quantum computers, while propagating light in optical fibers is ideal for communication between quantum processors. Small-scale quantum information processing has already been realized with various physical systems, such as superconducting qubits [3,4], trapped ions [5], electron spins in quantum dots [6], photonic qubits [7,8], and optical modes [9–11]. Furthermore, as for the creation of multimode entanglement which can be exploited as a resource in quantum computation and quantum networks, an ultra-large-scale entangled state with more than 10 000 entangled modes was recently reported [12].

Towards a physical implementation of a quantum computer, one approach is to make a network by connecting many quantum processors of moderate size. If local quantum operations at the nodes are combined with quantum communication between them, any quantum processing can be decomposed to a serial combination of local operations. In this case, the processors implement their local operations sequentially in time and use quantum channels or quantum teleporters [Fig. 1(a)] [13,14] to transmit quantum states among them. Quantum teleportation is advantageous compared to direct transfer of quantum states via quantum channels because, in the teleportation scenario, the teleportation fidelity can be brought close to unity by entanglement distillation [15] even when the connecting channel is lossy. In principle, a nonlocal quantum gate of an interaction operation $\hat{E}_{AB}$ between two nodes A and B is achievable with a sequence of three steps [Fig. 1(b)]: first teleporting a state from node A to node B, then locally coupling it with the other state present at node B by a local gate $\hat{E}_{AB}$, and finally teleporting one outcome from that gate operation back to node A [16].

Here we explore the possibility of reducing the above sequential and asymmetric three-step implementation to a parallel single-step implementation based on local operations and classical communication (LOCC) [Fig. 1(c)]. LOCC can never create an entangling gate; however, if LOCC is supported by entangled resource states shared in advance, this no-go theorem is irrelevant and a nonlocal entangling gate for arbitrary states may be implemented at the cost of consumption of the resource states. Indeed, the reduction is known to be possible for the most fundamental, controlled-NOT (CNOT) gate for qubit systems [17–19] and the quantum nondemolition (QND) gate for continuous variable (CV) systems [20,21]. The resulting speed-up means less decoherence, which is the main obstacle of quantum processing. Another advantage may be a symmetry of the parallel processing, allowing for balanced use of the processors. In practice, the resource entangled states shared in advance among nodes will be stored in quantum memories, but they can be retrieved at the time they are required and thus the subsequent implementation of the nonlocal gate itself can be deterministic within all-optical architecture, which is feasible with the current technology.

In this paper, we experimentally demonstrate the parallel implementation of a nonlocal QND gate within all-optical architecture, consuming minimal resources as schematized in Fig. 1(c), according to the proposal in Ref. [21]. We demonstrate a fundamental input-output relation which is characteristic of a QND gate. Furthermore, the nonlocal entangling nature of the gate can be verified by looking at the entanglement of the initially separable output states. Together with the previous test of CV quantum memories [22], our test opens a way towards the spatially distributed parallel CV processors.

II. THEORY

A. Nonlocal CNOT and QND gate

Distributed quantum computing was previously discussed for qubits [23,24]. It divides tasks into subroutines and executes them in parallel at several nodes of the quantum processor network. A parallel nonlocal gate is a nonlocal

*yokoyama@alice.t.u-tokyo.ac.jp
†akiraf@ap.t.u-tokyo.ac.jp

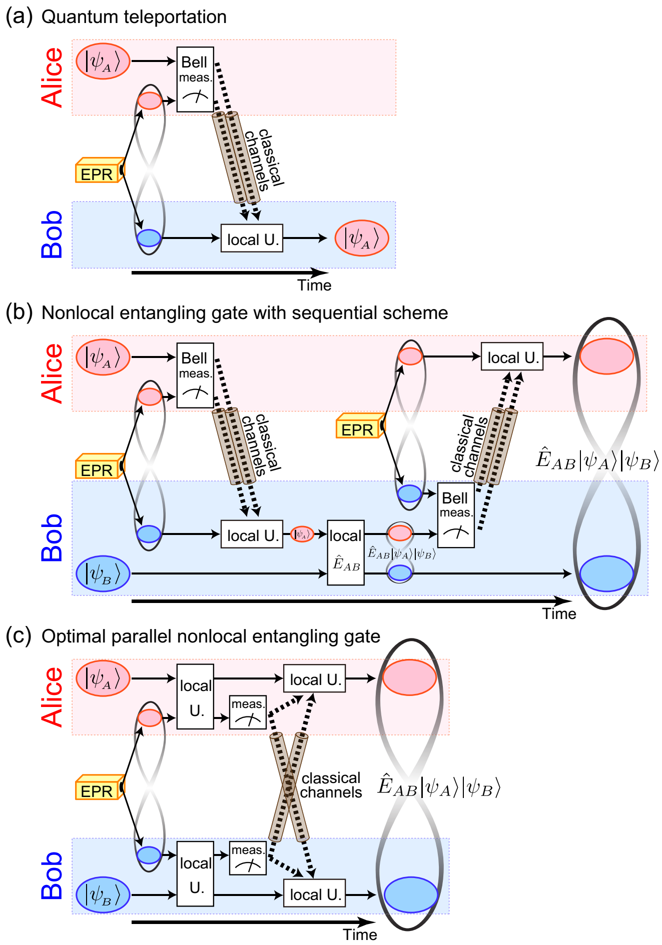

FIG. 1. (Color online) Abstract illustrations of some nonlocal gates. (a) Quantum teleportation from Alice to Bob. (b) Nonlocal entangling gate with sequential scheme by means of two quantum teleporters and one local entangling gate. (c) Optimal parallel nonlocal entangling gate. meas.: measurement; local U.: local unitary operation; EPR: entanglement resource; $\hat{E}_{AB}$: entangling operation for two input states.

extension of the teleportation of the local gate [25]. What are the minimal quantum resources required for implementation of a basic all-optical nonlocal gate? For qubits, the basic nonlocal CNOT gate ($\hat{C}_{AB}|a\rangle_A|b\rangle_B = |a\rangle_A|a+b \mod 2\rangle_B$, $a,b \in \{0,1\}$) can be principally implemented by one ebit of entanglement that is preshared between the nodes, two parallel local CNOT gates, two parallel local projective measurements, and two-way one-bit classical communication [17,18]. The practical application of the gates for distributed quantum computing has been discussed in Ref. [26]. Recently, the parallel implementation of the nonlocal CNOT gate has been discussed in detail [19]. The heralded but still probabilistic all-optical nonlocal CNOT gates in the parallel configuration were already implemented a long time ago [27,28].

For CV systems of quantum oscillators, an equivalent of the basic CNOT gate is a QND gate ($\hat{\Sigma}_{AB}|a\rangle_A|b\rangle_B = |a\rangle_A|a+b\rangle_B$, $a,b \in \mathbb{R}$) [10,20,21,29], which has been used as a main tool to make interactions in CV quantum information processing. Furthermore, the nondemolition measurement based on a local QND gate is a very important topic of quantum physics [30,31]. Advantageously, QND interaction naturally appears between light and atomic memories [22], and therefore the QND gate is a very good candidate for a constitutive gate in CV quantum processors. To test the principles of the basic QND gate, an all-optical realization of the local QND interaction for traveling beams has been constructed [29].

The nonlocal realization of the QND gate ($\hat{E}_{AB} = \hat{\Sigma}_{AB}$) in the parallel configuration and with minimal resources was actually suggested a long time ago [20]. For that nonlocal QND gate, the sufficient requirements are, in analogy with the case of the qubit CNOT gate, an Einstein-Podolsky-Rosen (EPR) state that is preshared between the nodes, two parallel local QND gates, two parallel homodyne projective measurements, and two parallel two-way classical communication of a real number [20]. Later, the parallel configuration of the nonlocal QND gate was theoretically extended to an all-optical realization where local operations are based on local beam-splitter gates instead of local QND gates [21], which is exactly what we experimentally demonstrate here. In this case, the QND gate is implemented up to *a priori* known local squeezing operations ($\hat{E}_{AB} = \hat{S}_A^\dagger \hat{S}_B \hat{\Sigma}_{AB}$, where $\hat{S}_k$ is a local squeezing operation, as explained later), which can be canceled by another local squeezing gate as already experimentally tested on traveling optical beams [9,32] or possibly implemented directly in atomic memories [33]. Note that the above implementations are not only composed of a smaller number of steps, but are also much less resource consuming compared to the teleportation-based sequential strategy [Fig. 1(b)], which consumes two EPR states and requires sequentially doubled two-way classical communication.

B. Nonlocal QND gate with minimal resources

We consider the scenario where two manipulators Alice and Bob, being separated by a large distance, would like to *simultaneously* apply a nonlocal QND sum gate onto their states by means of LOCC, supported by preprepared resource entangled states. We will consider the QND type of nonlocal deterministic sum gate described by the unitary transformation

$$\hat{\Sigma}_{AB} = e^{-2i\hat{x}_A\hat{p}_B}, \tag{1}$$

even though the considerations can be naturally extended to other nonlocal gates. Here $\hat{x}_j$ and $\hat{p}_j$, where $j = A,B$, denote the generalized position and momentum quadrature operators, which satisfy the commutation relation $[\hat{x}_j,\hat{p}_k] = i\delta_{jk}/2$ with $\hbar = 1/2$, where δ_{jk} is the Kronecker delta.

In Refs. [20,21], it was shown that one preshared maximally entangled state (ideal EPR state) and one ideal classical channel in each direction (two channels in total) are sufficient resources for the ideal deterministic nonlocal QND sum gate implemented in the parallel way for arbitrary input states owned by Alice and Bob. By the classical channel, we mean sending a classical real number $s \in \mathbb{R}$ over a distance. Is the maximally entangled state necessary to implement the nonlocal QND sum gate in the parallel way on both sides for all of the possible input states? The following answer is based on the well-known fact that the amount of entanglement cannot be increased by the deterministic LOCC operations [34]. The ideal EPR states are therefore necessary to be shared between Alice and Bob, since the QND sum gate is capable of creating an entangled state with an arbitrary large amount of entanglement from two pure separable states. For instance, when the initial quantum state owned by Alice is a momentum eigenstate $|p=0\rangle$ proportional to $\int |x\rangle dx$ while that owned by Bob is a position eigenstate $|x=0\rangle$, the output state after the gate operation becomes proportional to $\int |x\rangle_A \otimes |x\rangle_B dx$, which is the ideal EPR state containing an infinitely large amount of entanglement and infinitely large energy. Therefore, the ideal nonlocal QND sum gate can only be approached as the preshared CV entanglement between Alice and Bob infinitely increases.

To understand the role of classical communication in our procedure, we suppose that the initial state owned by Alice is a position eigenstate with an eigenvalue x_A and the state owned by Bob is another position eigenstate with an eigenvalue x_B. Since the nonlocal gate (1) implements $\hat{\Sigma}_{AB}|x_A\rangle_A \otimes |x_B\rangle_B = |x_A\rangle_A \otimes |x_B + x_A\rangle_B$, Bob could receive a classical real number x_A from Alice by comparing the position of his quantum state before and after the gate operation. Local operations cannot transmit classical information between Alice and Bob, even if they could exploit arbitrary preshared entanglement [35]. More specifically, the maximal classical information which can be transmitted via the nonlocal quantum gate is no more than the amount of classical information required in the implementation of the nonlocal gate. Thus Alice has to send at least one classical real number to Bob in order to implement the gate. In a similar way, when the initial states of Alice and Bob are eigenstates of momentum, Bob can transmit a classical real number to Alice via the nonlocal gate, which means Bob has to send at least one classical real number during the gate implementation. Consequently, they need at least one classical channel in each direction (two channels in total) for a nonlocal entangling gate, if it is based on LOCC and preshared entanglement.

On the other hand, if we could use high-fidelity quantum channels to directly transfer quantum states, we note that the sequential implementation requires less resources, as has been demonstrated in Refs. [20,21]. In principle, it requires only a single squeezed state (while an EPR state in the parallel scheme corresponds to two squeezed states) and a single one-way classical channel. However, the parallel scheme is still advantageous in the gate operation time. The time cost of communication is doubled for the sequential scheme: the sequential scheme requires, first, quantum communication from Alice to Bob *after the nonlocal gate operation is required*, and, second, classical communication from Bob to Alice *after the quantum communication is completed*, while the parallel scheme requires only two-way classical communication at once during the gate operation time because the resource EPR state can be shared *before the nonlocal gate operation is required*. In addition, the implementation based on preshared resource entanglement in principle enables entanglement distillation by coherently combining single-photon addition and subtraction operations [15,36,37] after they are transmitted through the quantum channels between Alice and Bob. From the discussions above, the advantage of the parallel scheme and the minimum resource for the gate implementation is intimately connected with the possibility to preshare quantum resources and to distill them, if the quantum channels are unreliable.

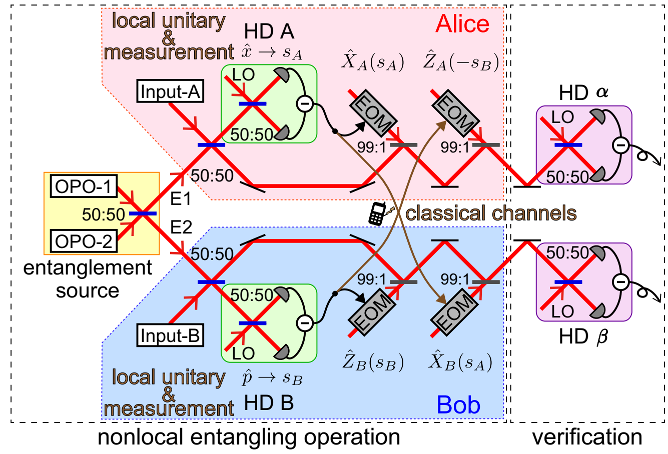

FIG. 2. (Color online) A schematic of our experimental setup. OPO: optical parametric oscillator; LO: local oscillator for homodyne measurement; EOM: electro-optical modulator; HD: homodyne detection; 50:50 (99:1): 50 (99)% reflectivity beam splitter.

C. Implementation of nonlocal QND gate

The procedure of the optimal nonlocal entangling gate consists of the following three key steps [21]. We will mathematically describe them by the transformations in the Heisenberg representation taking account of finite resource entanglement, which leads to a simple description for any input quantum state of the nonlocal gate. For comparison, the action of the QND gate for quadrature operators is

$$\hat{\boldsymbol{\xi}}'_{AB} = \hat{\Sigma}^{\dagger}_{AB}\hat{\boldsymbol{\xi}}_{AB}\hat{\Sigma}_{AB} = \begin{pmatrix} \hat{x}_A \\ \hat{p}_A - \hat{p}_B \\ \hat{x}_B + \hat{x}_A \\ \hat{p}_B \end{pmatrix}, \tag{2}$$

where $\hat{\boldsymbol{\xi}}'_{AB} = (\hat{x}'_A,\hat{p}'_A,\hat{x}'_B,\hat{p}'_B)^T$ and $\hat{\boldsymbol{\xi}}_{AB} = (\hat{x}_A,\hat{p}_A,\hat{x}_B,\hat{p}_B)^T$. By applying the gate, the position operator of Alice $\hat{x}_A$ is added to Bob's side $\hat{x}'_B = \hat{x}_B + \hat{x}_A$, while the momentum operator of Bob $\hat{p}_B$ is subtracted from Alice's side $\hat{p}'_A = \hat{p}_A - \hat{p}_B$ for the counteraction.

First, the EPR state is preshared by Alice and Bob before the gate is actually implemented. Note that its distribution does not reduce the speed of the gate. To approach the ideal EPR state with both infinite energy and entanglement, we use a realistic EPR entangled state, which can be experimentally generated by combining two finitely squeezed vacuum states on a balanced beam splitter, as is depicted in Fig. 2. The realistic EPR state with finite entanglement is characterized by two linear combinations of position and momentum operators as below:

$$\hat{x}_{E1} - \hat{x}_{E2} = \sqrt{2}\mathrm{e}^{-r}\hat{x}_1^{(0)}, \tag{3}$$

$$\hat{p}_{E1} + \hat{p}_{E2} = \sqrt{2}\mathrm{e}^{-r}\hat{p}_2^{(0)}. \tag{4}$$

Here, subscripts $E1$ and $E2$ denote two independent modes of an EPR state, while $e^{-r}\hat{x}_1^{(0)}$ and $e^{-r}\hat{p}_2^{(0)}$ are squeezed quadratures of the resource modes 1 and 2 before the balanced beam splitter combining, characterized by a squeezing parameter r, respectively. The limit $r \to \infty$ corresponds to the ideal EPR state.

Second, Alice and Bob couple their own input states (A and B, respectively) with the shared EPR state on their local balanced beam splitters. Then, one of the outputs on each side is measured by means of homodyne detection, making the projection on the eigenstate of either position or momentum variable. The chosen measured observables correspond to

$$\hat{x}_{E1'} = \frac{1}{\sqrt{2}}(\hat{x}_A - \hat{x}_{E1}) \quad \text{and} \quad \hat{p}_{E2'} = \frac{1}{\sqrt{2}}(\hat{p}_B - \hat{p}_{E2}), \quad (5)$$

and the measurement outcomes from them are denoted by s_A and s_B in the following, respectively. On the other hand, the quadratures of the remaining parts are

$$\hat{x}_{A'} = \frac{1}{\sqrt{2}}(\hat{x}_A + \hat{x}_{E1}), \quad \hat{p}_{A'} = \frac{1}{\sqrt{2}}(\hat{p}_A + \hat{p}_{E1}), \quad (6)$$

$$\hat{x}_{B'} = \frac{1}{\sqrt{2}}(\hat{x}_B + \hat{x}_{E2}), \quad \hat{p}_{B'} = \frac{1}{\sqrt{2}}(\hat{p}_B + \hat{p}_{E2}). \quad (7)$$

Third, the measurement outcomes are transmitted to the other party through a two-way classical channel. According to the measurement outcomes, both Alice and Bob perform feed-forward operations expressed by the operator $\hat{X}_{A'}(s_A)\hat{Z}_{A'}(-s_B)\hat{X}_{B'}(s_A)\hat{Z}_{B'}(s_B)$ on the rest of their states, where $\hat{X}_k(s) = e^{-2is\hat{p}_k}$ and $\hat{Z}_k(s) = e^{2is\hat{x}_k}$ are position and momentum displacement operators on modes $k = A', B'$, respectively. Consequently, the input-output relation is given by

$$\hat{\boldsymbol{\xi}}_{\alpha\beta} = \begin{pmatrix} \sqrt{2} & 0 & 0 & 0 \\ 0 & \frac{1}{\sqrt{2}} & 0 & -\frac{1}{\sqrt{2}} \\ \frac{1}{\sqrt{2}} & 0 & \frac{1}{\sqrt{2}} & 0 \\ 0 & 0 & 0 & \sqrt{2} \end{pmatrix} \hat{\boldsymbol{\xi}}_{AB} + \hat{\boldsymbol{\delta}} \quad (8)$$

$$\equiv \hat{E}^{\dagger}_{AB}\hat{\boldsymbol{\xi}}_{AB}\hat{E}_{AB} + \hat{\boldsymbol{\delta}}, \quad (9)$$

where $\hat{\boldsymbol{\xi}}_{AB} = (\hat{x}_A, \hat{p}_A, \hat{x}_B, \hat{p}_B)^T$, $\hat{\boldsymbol{\xi}}_{\alpha\beta} = (\hat{x}_\alpha, \hat{p}_\alpha, \hat{x}_\beta, \hat{p}_\beta)^T$, $\hat{\boldsymbol{\delta}} = (0, \mathrm{e}^{-r}\hat{p}_2^{(0)}, \mathrm{e}^{-r}\hat{x}_1^{(0)}, 0)^T$, and $\hat{E}_{AB}$ is the entangling operator. We use indices A,B for the input modes and α,β for the output modes. In the limit of infinite squeezing $r \to \infty$, the contribution of $\hat{\boldsymbol{\delta}}$ from the preshared state vanishes and the gate operation reaches a perfect unitary operation.

The obtained interaction operator $\hat{E}_{AB}$ can be decomposed into $\hat{E}_{AB} = \hat{S}^{\dagger}_A \hat{S}_B \hat{\Sigma}_{AB}$, where $\hat{S}_j = e^{i \ln 2(\hat{x}_j\hat{p}_j + \hat{p}_j\hat{x}_j)/2}$ denotes the -3.0 dB, x-squeezing operator on mode j. Note that local unitary operations do not consume nonlocal resources and do not change the amount of entanglement between the two systems. In this sense, our nonlocal gate $\hat{E}_{AB}$ is equivalent to a nonlocal QND sum gate $\hat{\Sigma}_{AB}$. The additional local squeezing is explained from the fact that the measurement-induced input coupling with the balanced beam splitter works as a universal squeezer with the squeezing level of -3.0 dB [9,21]. It is a difference from the implementation based on the local QND interactions [20], for which the nonlocal QND is obtained without any local corrections. If it is necessary, the additional local squeezing can be corrected optically by the universal squeezers [9,21] or it can be eliminated in the quantum memory [33].

Up to the residual local squeezing, the implemented nonlocal QND interaction is

$$\hat{\Sigma}^{\dagger}_{AB}\hat{\boldsymbol{\xi}}_{AB}\hat{\Sigma}_{AB} + \hat{\boldsymbol{\eta}}, \quad (10)$$

where $\hat{\boldsymbol{\eta}} = (0, \sqrt{2}e^{-r}\hat{p}_2^{(0)}, \sqrt{2}e^{-r}\hat{x}_1^{(0)}, 0)^T$. The residual noise existing in $\hat{p}_\alpha$ and $\hat{x}_\beta$ variables can be reduced by sufficient squeezing from the squeezers OPO-1 and OPO-2, depicted in Fig. 2. Advantageously, the feed-forward corrections eliminate the noise existing in the antisqueezed quadratures $\hat{p}_1^{(0)}e^r$ and $\hat{x}_2^{(0)}e^r$, and therefore an impurity of the squeezed states from the OPO-1 and OPO-2 is not limiting. The application of the high squeezing stimulates further experimental investigation of the limits of optical squeezing generated from the modern optical parametric oscillators [38,39].

The scheme is also advantageous in the sense of the efficient use of arbitrary weak resource squeezing from OPO-1 and OPO-2. To demonstrate this, we consider the case where both input states are coherent states. Since Eq. (9) is linear in position and momentum operators, the output state becomes a Gaussian state. The first moments do not affect the amount of entanglement and thus we can solely concentrate on the second central moments which are uniquely described by the covariance matrix given by $V \equiv \frac{1}{2}\langle\{\hat{\boldsymbol{\xi}}, \hat{\boldsymbol{\xi}}\}\rangle$, where $\{\hat{\boldsymbol{u}}, \hat{\boldsymbol{v}}\} \equiv \hat{\boldsymbol{u}}\hat{\boldsymbol{v}}^T + (\hat{\boldsymbol{v}}\hat{\boldsymbol{u}}^T)^T$ [40]. Logarithmic negativity E_N is a good indicator of Gaussian entanglement, invariant under local unitary operations [41,42]. For a Gaussian state, the logarithmic negativity can be calculated from its covariance matrix [43]. In our case, the covariance matrix and the logarithmic negativity are as follows:

$$V_{\alpha\beta} = \frac{1}{4}\begin{pmatrix} 2 & 0 & 1 & 0 \\ 0 & 1+e^{-2r} & 0 & -1 \\ 1 & 0 & 1+e^{-2r} & 0 \\ 0 & -1 & 0 & 2 \end{pmatrix}, \quad (11)$$

$$E_N = -\ln[\sqrt{2(1+e^{-2r})} - 1]. \quad (12)$$

Note that the local squeezing unitary operations potentially used to obtain the exact QND form of the nonlocal interaction do not change the amount of generated entanglement. From Eq. (12), we know that E_N is always positive, which means inseparability of the two subsystems even if the resource squeezing is infinitesimal. This fact highlights the efficiency of our scheme in comparison with Ref. [10]. In fact, the recent report of a one-way scheme with a four-mode linear cluster state [10] can also be regarded as a nonlocal CV gate; however, that gate not only requires four single-mode squeezed resource states instead of the two demonstrated here, but also the resource squeezing level of more than -4.0 dB in order to obtain an entangled output state from two coherent inputs.

III. EXPERIMENTAL SETUP

The schematic of our experimental setup is shown in Fig. 2. The light source is a continuous-wave Ti:sapphire laser with a wavelength of 860 nm and a power of about 1.7 W. The quantum states to be processed are in optical modes at 1 MHz sidebands of the laser beam.

The resource EPR beams are prepared by combining two squeezed vacuum states on a 50% reflectivity beam splitter. The two squeezed vacuum states are each generated by a subthreshold optical parametric oscillator (OPO). The OPO is a bowtie-shaped cavity with a round-trip length of 500 mm, containing a periodically poled $KTiOPO_4$ (PPKTP) crystal with 10 mm in length as a nonlinear medium [44]. A second harmonic light beam with wavelength of 430 nm and power of about 80 mW pumps each OPO, which is generated by another bowtie-shaped cavity containing a $KNbO_3$ crystal as a nonlinear medium (omitted in Fig. 2). Squeezing levels of the resource squeezed vacuum states are about −4 dB relative to the shot-noise level.

Nonzero amplitude of an input coherent state at 1 MHz sidebands is generated by modulating the phase of the optical carrier with a piezoelectric transducer (PZT) at 1 MHz. The phase modulation creates a sideband coherent amplitude which is out of phase with the optical carrier, and we can use it as an excitation in either the $\hat{x}$ or $\hat{p}$ quadrature of the input coherent state by controlling the phase of the optical carrier entering the QND gate. Input coupling with one of the EPR beams at each party is achieved via a 50% reflectivity beam splitter. Then, one of the two beams in each party is measured by a homodyne detector. The measurement outcomes are sent to the other party, where they are used to drive suitable displacement operations. A displacement operation is achieved by combining the main beam, which carries the quantum state to be displaced at 1 MHz, with an auxiliary beam, which is modulated at 1 MHz on a 99% reflectivity beam splitter. The auxiliary beam is modulated by an electro-optic modulator (EOM), to which the homodyne signal is sent after adjusting the gain and the phase at 1 MHz by electronic circuits.

In order to characterize the input and output states of the gate, we measure powers of the quadratures with a spectral analyzer. The measurement frequency is 1 MHz, while the resolution and video bandwidths are 30 kHz and 300 Hz, respectively. The data are averaged 20 times.

The propagation losses from the OPOs to the homodyne detectors are 3% to 10%. The detectors' quantum efficiencies are 99%. The interference visibilities are 97% on average.

IV. EXPERIMENTAL RESULTS

We have collected our experimental results testing the nonlocal QND sum gate up to the local squeezing operations as shown in Figs. 3 and 4. Figure 3 shows the output quadrature powers for several input coherent states, from which the input-output relation is confirmed. Figure 4 shows a covariance matrix of one of the output Gaussian states, from which the existence of entanglement is verified.

First, we determine variances of the output quadratures by checking the case of vacuum input states and depict them in Fig. 3(a). The theoretical predictions and experimental results are shown in Fig. 3(a). The ideal case, which corresponds to $r \to \infty$ in Eq. (9), is shown by cyan lines. On one hand, the uncorrelated quantum fluctuations of $\hat{p}_B$ and $\hat{x}_A$ are added to those of $\hat{p}_A$ and $\hat{x}_B$ by the sum gate $\hat{E}_{AB}$, which leads to 3.0 dB increase of $\hat{p}_A$ and $\hat{x}_B$. On the other hand, additional local squeezing operation $\hat{S}_A^\dagger \hat{S}_B$ increases $\hat{x}_A$ and $\hat{p}_B$ by 3.0 dB, while it decreases $\hat{p}_A$ and $\hat{x}_B$. In total, at the output of the gate, the variances of $\hat{p}_\alpha$ and $\hat{x}_\beta$ are equal to the shot-noise level (SNL), while the variances of $\hat{x}_\alpha$ and $\hat{p}_\beta$ are 3.0 dB above the SNL (two times the SNL).

When the resource squeezing in the OPO-1 and OPO-2 is finite, the output states are influenced by the additional excess noise. We show as a reference the theoretical prediction for the case without the entanglement [$r = 0$ in Eq. (9)] by green dashed lines. In this case, the nonlocal operation is performed purely classically, assisted only by the two-way classical communication. The variances of $\hat{p}_\alpha$ and $\hat{x}_\beta$ become 3.0 dB above the SNL (two times the SNL), while those of $\hat{x}_\alpha$ and $\hat{p}_\beta$ are not affected by the level of resource squeezing. The experimental results of $\langle \hat{x}_\alpha^2 \rangle$, $\langle \hat{p}_\alpha^2 \rangle$, $\langle \hat{x}_\beta^2 \rangle$, and $\langle \hat{p}_\beta^2 \rangle$, shown by the red traces, are between the cyan and green lines due to the finite resource squeezing. They correspond to 3.0, 1.2, 1.5, and 3.1 dB above the SNL from left to right, respectively. These results are consistent with the resource squeezing level of −4 dB, which leads to 1.5 dB above the SNL for $\hat{p}_\alpha$ and $\hat{x}_\beta$.

Second, we replace the input vacuum state of either mode A or mode B by a coherent state, by which the input-output relation is confirmed on the assumption of linear response of

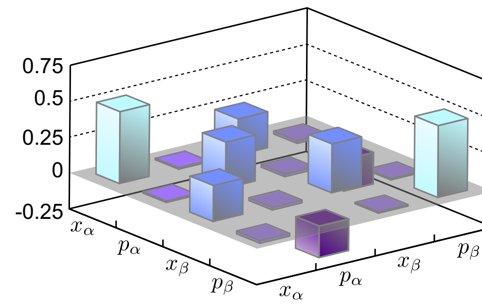

FIG. 4. (Color online) A covariance matrix of output states for vacuum inputs. Measured values of the covariance matrix are shown in Eq. (13).

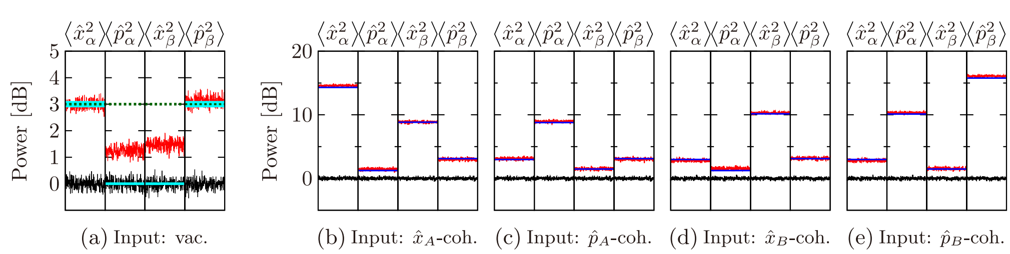

FIG. 3. (Color online) (a) Powers at the outputs for vacuum inputs. The black and red traces show the shot noise and experimental output quadratures, respectively. The green dashed lines show the theoretical predictions without resource squeezing, while the cyan lines show the theoretical predictions for an ideal gate. (b)–(e) Powers at the outputs for coherent inputs where $(\langle \hat{x}_A \rangle, \langle \hat{p}_A \rangle, \langle \hat{x}_B \rangle, \langle \hat{p}_B \rangle)$ corresponds to $(a,0,0,0)$, $(0,a,0,0)$, $(0,0,b,0)$, and $(0,0,0,b)$, respectively. The coherent amplitudes a and b correspond to 11.0 and 12.5 dB above the shot-noise level, respectively. The blue lines show the theoretical predictions based on the experimental results of (a). vac.: vacuum state; coh.: coherent state.

the gate. The powers of the input amplitude quadratures are individually measured in advance, corresponding to 11.0 dB for mode A and 12.5 dB for mode B, respectively, compared to the SNL. Figure 3(b) shows the powers of the output quadratures as red traces when the input A is in a coherent state with a nonzero coherent amplitude only in the $\hat{x}_A$ quadrature. It corresponds to 11.0 dB above the SNL, while the input B is in a vacuum state. We observe an increase in power of $\hat{x}_\alpha$ and $\hat{x}_\beta$ compared to the case of two vacuum inputs, which is caused by the nonzero coherent amplitude. On the other hand, $\hat{p}_\alpha$ and $\hat{p}_\beta$ are not changed. In the same figure, the theoretical prediction calculated from the measured input coherent amplitude is shown by blue lines. Due to the additional local squeezing operators $\hat{S}_A^\dagger \hat{S}_B$, the coherent power of $\hat{x}_\alpha$ increases by 3.0 dB (corresponding to about 14 dB above the SNL), while that of $\hat{x}_\beta$ decreases by 3.0 dB (corresponding to about 8 dB above the SNL), respectively. Similarly, Figs. 3(c)–3(e) show the results with a nonzero coherent amplitude in the $\hat{p}_A$, $\hat{x}_B$, and $\hat{p}_B$ quadratures, respectively.

These experimental results are in good agreement with the theory described by the transformation (9). We see the expected feature of the sum gate that the sum of $\hat{x}_A$ and $\hat{x}_B$ appears in $\hat{x}_\beta$, while the sum of $\hat{p}_A$ and $-\hat{p}_B$ appears in $\hat{p}_\alpha$, up to the local squeezing. We believe that the small discrepancies between our experimental results and the theoretical predictions are caused by the (unbalanced) propagation losses and nonunity visibilities of interferences with local oscillators at the homodyne detections.

Finally, Fig. 4 shows the covariance matrix of the output state, calculated from the experimental variances for the case of the vacuum input states. The diagonal elements are obtained by measuring the variances of the output quadratures $\hat{x}_j$ and $\hat{p}_j$. The off-diagonal elements in each single mode, such as V_{12}, are obtained by measuring the variances of $(\hat{x}_j \pm \hat{p}_j)/\sqrt{2}$. The other off-diagonal elements can be obtained by measuring the variances of $\hat{\xi}_j \pm \hat{\xi}_k$, where $\hat{\xi} = \{\hat{x}, \hat{p}\}$. The experimental covariance matrix is as follows:

$$V = \begin{pmatrix} 0.50 & 0.01 & 0.25 & -0.02 \\ 0.01 & 0.32 & -0.02 & -0.22 \\ 0.25 & -0.02 & 0.34 & -0.01 \\ -0.02 & -0.22 & -0.01 & 0.50 \end{pmatrix}. \qquad (13)$$

The margin of error for each measured matrix element is plus or minus less than 0.002. Note that it satisfies the physical condition $V + (i/4)\ \Omega \geqslant 0$, where $\Omega = \begin{pmatrix} 0 & -1 \\ 1 & 0 \end{pmatrix} \oplus \begin{pmatrix} 0 & -1 \\ 1 & 0 \end{pmatrix}$ [43,45]. The covariance matrix obtained from the measurement results is in good agreement with the theoretical prediction in Eq. (11). We then calculate the logarithmic negativity E_N of the output state from this covariance matrix by using Eq. (13), and the obtained value is

$$E_N = 0.40 \pm 0.01. \qquad (14)$$

This value corresponds to -4.1 ± 0.1 dB from Eq. (12), which is in good agreement with the experimental resource squeezing level of about -4 dB. The nonzero (positive) value is the evidence of the entanglement between the two output modes.

V. CONCLUSION

We have experimentally demonstrated an all-optical nonlocal QND sum gate for continuous variables up to local squeezing unitary operations. Advantageously, this all-optical scheme needs only local passive beam-splitter coupling between the optical modes at each node. It also requires one preshared state with the EPR quantum correlations and one two-way classical channel, which are the minimal resource requirements for a nonlocal entangling QND gate. In our experiment, all of the local operations, measurements, and two-way classical communications are running truly in parallel, which increases the speed of the gate to the limit given by the technical issues. The capability of the gate to produce entanglement at the output is verified by the logarithmic negativity for the case of two coherent input states. The nonlocal all-optical QND gate, together with quantum memories, can be, in the future, incorporated into distributed quantum computing as a cross-processor operation.

ACKNOWLEDGMENTS

This work was partly supported by PDIS, GIA, APSA commissioned by the MEXT of Japan, and FIRST initiated by CSTP, ASCR-JSPS, and the SCOPE program of the MIC of Japan. S.Y. acknowledges support from ALPS. R.U. acknowledges support from JSPS. P.M. acknowledges support from Grant No. P205/12/0577 of the Czech Science Foundation and R.F. acknowledges the support of the Czech-Japan bilateral grant of MSMT CR, Grant No. LH13248 (KONTAKT).

[1] M. A. Nielsen and I. L. Chuang, *Quantum Computation and Quantum Information* (Cambridge University Press, Cambridge, UK, 2000).

[2] A. Furusawa and P. van Loock, *Quantum Teleportation and Entanglement: A Hybrid Approach to Optical Quantum Information Processing* (Wiley-VCH Verlag GmbH KGaA, Germany, 2011).

[3] L. Dicarlo, J. M. Chow, J. M. Gambetta, Lev S. Bishop, B. R. Johnson, D. I. Schuster, J. Majer, A. Blais, L. Frunzio, S. M. Girvin, and R. J. Schoelkopf, Nature (London) **460**, 240 (2009).

[4] T. Yamamoto, M. Neeley, E. Lucero, R. C. Bialczak, J. Kelly, M. Lenander, M. Mariantoni, A. D. O'Connell, D. Sank, H. Wang, M. Weides, J. Wenner, Y. Yin, A. N. Cleland, and J. M. Martinis, Phys. Rev. B **82**, 184515 (2010).

[5] B. P. Lanyon, C. Hempel, D. Nigg, M. Muller, R. Gerritsma, F. Zahringer, P. Schindler, J. T. Barreiro, M. Rambach, G. Kirchmair, M. Hennrich, P. Zoller, R. Blatt, and C. F. Roos, Science **334**, 57 (2011).

[6] F. H. L. Koppens, C. Buizert, K. J. Tielrooij, I. T. Vink, K. C. Nowack, T. Meunier, L. P. Kouwenhoven, and L. M. K. Vandersypen, Nature (London) **442**, 766 (2006).

[7] X.-C. Yao, T.-X. Wang, H.-Z. Chen, W.-B. Gao, A. G. Fowler, R. Raussendorf, Z.-B. Chen, N.-L. Liu, C.-Y. Lu, Y.-J. Deng, Y.-A. Chen, and J.-W. Pan, Nature (London) **482**, 489 (2012).

[8] X.-Q. Zhou, P. Kalasuwan, T. C. Ralph, and J. L. O'Brien, Nat. Photon. **7**, 223 (2013).

[9] J. Yoshikawa, T. Hayashi, T. Akiyama, N. Takei, A. Huck, U. L. Andersen, and A. Furusawa, Phys. Rev. A **76**, 060301(R) (2007).

[10] R. Ukai, S. Yokoyama, J. Yoshikawa, P. van Loock, and A. Furusawa, Phys. Rev. Lett. **107**, 250501 (2011).

[11] X. Su, S. Hao, X. Deng, L. Ma, M. Wang, X. Jia, C. Xie, and K. Peng, Nat. Commun. **4**, 2828 (2013).

[12] S. Yokoyama, R. Ukai, S. C. Armstrong, C. Sornphiphatphong, T. Kaji, S. Suzuki, J. Yoshikawa, H. Yonezawa, N. C. Menicucci, and A. Furusawa, Nat. Photon. **7**, 982 (2013).

[13] L. Vaidman, Phys. Rev. A **49**, 1473 (1994).

[14] S. L. Braunstein and H. J. Kimble, Phys. Rev. Lett. **80**, 869 (1998).

[15] H. Takahashi, J. S. Neergaard-Nielsen, M. Takeuchi, M. Takeoka, K. Hayasaka, A. Furusawa, and M. Sasaki, Nat. Photon. **4**, 178 (2010).

[16] H. Yonezawa, A. Furusawa, and P. van Loock, Phys. Rev. A **76**, 032305 (2007).

[17] J. Eisert, K. Jacobs, P. Papadopoulos, and M. B. Plenio, Phys. Rev. A **62**, 052317 (2000).

[18] B. Reznik, Y. Aharonov, and B. Groisman, Phys. Rev. A **65**, 032312 (2002).

[19] L. Yu, R. B. Griffiths, and S. M. Cohen, Phys. Rev. A **85**, 012304 (2012).

[20] R. Filip, Phys. Rev. A **69**, 052313 (2004).

[21] R. Filip, P. Marek, and U. L. Andersen, Phys. Rev. A **71**, 042308 (2005).

[22] B. Julsgaard, J. Sherson, J. I. Cirac, Jaromir Fiurasek, and E. S. Polzik, Nature (London) **432**, 482 (2004).

[23] J. I. Cirac, A. K. Ekert, S. F. Huelga, and C. Macchiavello, Phys. Rev. A **59**, 4249 (1999).

[24] H. K. Lo, Phys. Rev. A **62**, 012313 (2000).

[25] S. D. Bartlett and W. J. Munro, Phys. Rev. Lett. **90**, 117901 (2003).

[26] L. Jiang, J. M. Taylor, A. S. Sorensen, and M. D. Lukin, Phys. Rev. A **76**, 062323 (2007).

[27] S. Gasparoni, J.-W. Pan, Ph. Walther, T. Rudolph, and A. Zeilinger, Phys. Rev. Lett. **93**, 020504 (2004).

[28] Y.-F. Huang, X.-F. Ren, Y.-S. Zhang, L.-M. Duan, and G.-C. Guo, Phys. Rev. Lett. **93**, 240501 (2004).

[29] J. Yoshikawa, Y. Miwa, A. Huck, U. L. Andersen, P. van Loock, and A. Furusawa, Phys. Rev. Lett. **101**, 250501 (2008).

[30] P. Grangier, J. A. Levenson, and J. P. Poizat, Nature (London) **396**, 537 (1998).

[31] R. J. Sewell, M. Napolitano, N. Behbood, G. Colangelo, and M. W. Mitchell, Nat. Photon. **7**, 517 (2013).

[32] Y. Miwa, J. Yoshikawa, N. Iwata, M. Endo, P. Marek, R. Filip, P. van Loock, and A. Furusawa, Phys. Rev. Lett. **113**, 013601 (2014).

[33] R. Filip, Phys. Rev. A **78**, 012329 (2008).

[34] M. A. Nielsen, Phys. Rev. Lett. **83**, 436 (1999).

[35] A. Peres and D. R. Terno, Rev. Mod. Phys. **76**, 93 (2004).

[36] J. Fiurášek, Phys. Rev. A **82**, 042331 (2010).

[37] Y. Kurochkin, A. S. Prasad, and A. I. Lvovsky, Phys. Rev. Lett. **112**, 070402 (2014).

[38] Y. Takeno, M. Yukawa, H. Yonezawa, and A. Furusawa, Opt. Express **15**, 4321 (2007).

[39] M. Mehmet, H. Vahlbruch, N. Lastzka, K. Danzmann, and Roman Schnabel, Phys. Rev. A **81**, 013814 (2010).

[40] N. C. Menicucci, S. T. Flammia, and P. van Loock, Phys. Rev. A **83**, 042335 (2011).

[41] G. Vidal and R. F. Werner, Phys. Rev. A **65**, 032314 (2002).

[42] M. B. Plenio, Phys. Rev. Lett. **95**, 090503 (2005).

[43] S. Pirandola, A. Serafini, and S. Lloyd, Phys. Rev. A **79**, 052327 (2009).

[44] S. Suzuki, H. Yonezawa, F. Kannnari, M. Sasaki, and A. Furusawa, Appl. Phys. Lett. **89**, 061116 (2006).

[45] R. Simon, N. Mukunda, and B. Dutta, Phys. Rev. A **49**, 1567 (1994).